Diamond & Related Materials 20 (2011) 299–303

Contents lists available at ScienceDirect

Diamond & Related Materials

journal homepage: www.elsevier.com/locate/diamond

Cross-sectional structural analysis of C_{60} nanowhiskers by transmission electron microscopy

Ryoei Kato, Kun'ichi Miyazawa *

Fullerene Engineering Group, Exploratory Nanotechnology Research Laboratory, National Institute for Materials Science, 1-1, Namiki, Tsukuba, Ibaraki 305-0044, Japan

ARTICLE INFO

Article history:
Received 9 September 2010
Received in revised form 17 November 2010
Accepted 9 January 2011
Available online xxxx

Keywords:
Fullerene nanowhiskers
C_{60} nanowhiskers
Fullerene
Liquid–liquid interfacial precipitation method (LLIP)
Cross-section

ABSTRACT

Cross-sectional observations of C_{60} nanowhiskers (C_{60}NWs) were successfully conducted using the focused ion beam (FIB) method. The C_{60}NWs were observed to possess the core-shell structures with porous cores and dense surface thin layers. The size and number of pores decreased from the center to the surface, showing that the densification of C_{60}NWs proceeds from the surface to the center upon drying. A cross-sectional high-resolution transmission electron microscopy (HRTEM) image of a C_{60}NW showed a disordered structure comprising the domains with sizes on the order of 10 nm. The most frequently observed cross-sections were hexagons, reflecting the solvated hexagonal crystal structures of as-grown C_{60}NWs. From the observation of various cross-sectional shapes of C_{60}NWs with different diameters and crystallographic surface analysis, it is suggested that C_{60}NWs grow longer above a critical diameter D_c with the development of low-energy crystal surfaces.

1. Introduction

It has been known that the needle-like crystals of C_{60}, "C_{60} whiskers," exhibit anomalous properties depending on their diameter. Firstly, the electrical resistivity of C_{60} whiskers rapidly decreases with decreasing diameter [1,2], and secondly, the Young's modulus of C_{60} whiskers increases with decreasing diameter [3]. Since these anomalous properties are considered to be caused by some structural inhomogeneity along the radial direction of the whiskers, detailed cross-sectional structural investigations are necessary.

Up to now, the cross-sectional observations of C_{60} whiskers have been performed by using thin sliced samples prepared using microtome [1,4]. Our former observations showed that C_{60} whiskers were composed of thin slabs with a thickness of about 10 nm [5], and a high density of (111) stacking faults were observed in a cross-section of a C_{60} whisker that was prepared with a microtome [4].

Although the cross-sections of C_{60} whiskers with a thickness greater than 1 μm showed clear {111} crystal surfaces in Fig. 4 [1] and Fig. 7 [4], the other crystal surfaces were not well characterized owing to their irregular surface morphologies.

The determination of cross-sectional shapes of C_{60} whiskers is important. For example, the geometrical moment of inertia used in the measurement of their Young's modulus by bending testing in a transmission electron microscope (TEM) depends on the cross-sectional shape of the C_{60} whiskers [3,6,7].

Although the microtome technique is often used in preparing cross-sectional samples using a suitable glue to embed the samples, shear stresses are inevitably imposed on the samples. The shear stress may introduce lattice defects such as stacking faults and dislocations. The high-density stacking faults observed in the above cross-sectional images of C_{60} whiskers may have been introduced by the sample preparation process with a microtome.

On the other hand, the focused ion beam (FIB) is a powerful tool to prepare thin-foil samples for TEM observation [8]. The FIB method makes it possible to obtain thin-foil samples with desired thicknesses at selected sample locations, although some artifacts like dislocations and amorphous surface layers may be introduced owing to the high-energy ion sources [9,10]. The present study has been performed as the first trial to observe the cross-sectional samples of C_{60} whiskers prepared by the FIB method. "C_{60} nanowhiskers (C_{60}NWs)," C_{60} whiskers with diameters smaller than 1 μm, have been investigated, since they exhibit higher Young's moduli and lower electrical resistivities than thicker C_{60} whiskers [1–3].

2. Experimental procedure

C_{60}NWs were fabricated by the liquid–liquid interfacial precipitation method (LLIP method) using good solvent solutions such as pyridine, benzene and toluene saturated with C_{60} (MTR Ltd. 99.5% pure) and isopropyl alcohol (IPA) as a poor solvent [11–13].

As shown in Fig. 1, the C_{60}NWs were placed on a thin layer of polyvinyl alcohol (PVA) deposited on a Si substrate. The second PVA layer was carefully deposited on the C_{60}NWs to be able to locate the sample position for thinning by a scanning electron microscope (SEM)

* Corresponding author. Tel./fax: +81 29 860 4667.
E-mail address: miyazawa.kunichi@nims.go.jp (K. Miyazawa).

0925-9635/$ – see front matter © 2011 Elsevier B.V. All rights reserved.
doi:10.1016/j.diamond.2011.01.016

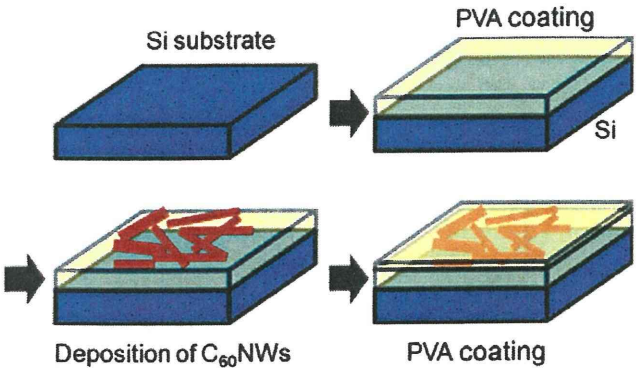

Fig. 1. The process used to prepare the sample with C_{60}NWs dispersed in a PVA film coated on a silicon substrate.

attached to an FIB system (Hitachi, FB-2100). Fig. 2 (a) and (b) show optical microscopy and SEM images of the embedded C_{60}NWs located at the same position on the sample. Since the second PVA layer was thin enough, traces of C_{60}NWs observed in the optical microscopy image could be recognized by the SEM of the FIB system and were easily subjected to the thinning process by the Ga ion source (15–40 keV, 0.01–2.8 nA) after depositing a protective tungsten (W) film. The cross-sectional morphology and structure of the C_{60} whiskers were observed by TEM (200 kV, JEOL JEM-2010).

3. Results and discussion

A typical cross-sectional TEM image for the sample thinned by FIB is shown in the TEM image of Fig. 3 (a). Fig. 3 (b) is a side view SEM image of Fig. 3 (a), showing a thin foil with an edge thickness of about 240 nm. The top part of the sample shows a tungsten layer that was used as a protective coating layer in the FIB process. Among the five cross-sectional images (A–E), images A, B and C show clear hexagonal shapes, reflecting the hexagonal crystal structure of as-grown solvated C_{60} whiskers [14]. The diameter of whisker C is about 1 μm. The whiskers A, B, D and E have diameters less than 1 μm and are normally called "C_{60} nanowhiskers" as described above [15]. Although whiskers A and B have similar diameters and contain tiny pores inside (Fig. 4 (a)), whisker B shows an exceptionally large pore near its center. The formation of such a large pore indicates inhomogeneous densification of the solvated matrix. A circumcircle defined for the cross-section A of Fig. 4 (a) is shown in Fig. 4 (b).

Fig. 5 (a) shows a histogram of pore diameters measured for the cross-section of whisker A of Fig. 4 (a). Regarding the pore as an ellipse, the pore diameter was calculated as the average value between the major axis and the minor axis. The average pore size was calculated to be 8.3 ± 2.3 nm. The maximum pore diameter was observed to be about 19 nm. Fig. 5 (b) shows that the pore diameter becomes smaller near to the whisker surface, although the pore diameter shows a large scatter between ~5 nm and ~20 nm. As shown in Fig. 5 (c), the distance between the pores and the whisker center O was measured and expressed as a histogram. Using this radial distribution of pore-to-center distances, the area number density of pores per square micrometer was plotted as a function of the radial distance (Fig. 5 (d)). It was observed that the area number density of pores ranged from about 1000–2500 μm^{-2} within a radius of 150 nm from the whisker center and rapidly decreased towards the surface. Hence, the C_{60}NW A was found to have a core-shell structure with a porous core and dense surface layer. Taking the maximum radius of the porous region to be about 240 nm, the thickness of the dense surface shell was calculated to be about 150 nm. In addition, it is clear that the densification of C_{60}NWs proceeds from the surface to the center by drying. The anomalous mechanical and electrical properties of C_{60} whiskers that depend on the whisker diameter must be caused by the existence of porous cores. In the synthesis of C_{60}NWs using a

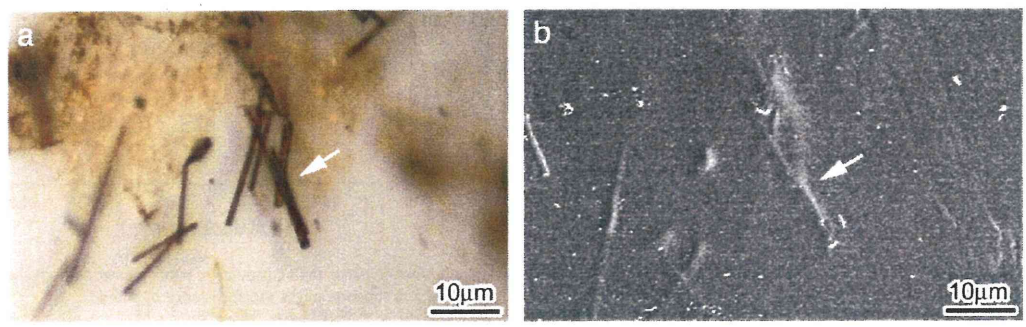

Fig. 2. (a) Optical microscopy image of the C_{60}NWs embedded in a PVA film and (b) SEM image of the area indicated by the arrow in (a). The C_{60}NWs were prepared by a C_{60}-saturated pyridine/IPA solution.

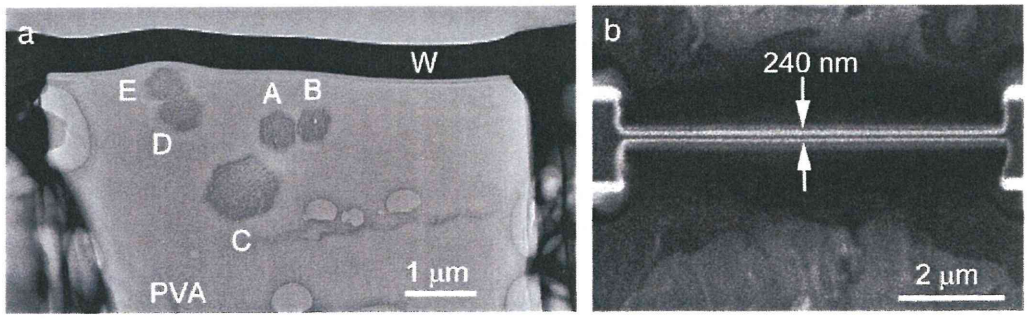

Fig. 3. (a) Cross-sectional TEM image of C_{60} whiskers embedded in a PVA film. The tungsten coating layer is shown by W. (b) Side-view SEM image for cross-section (a) with an edge thickness of 240 nm.

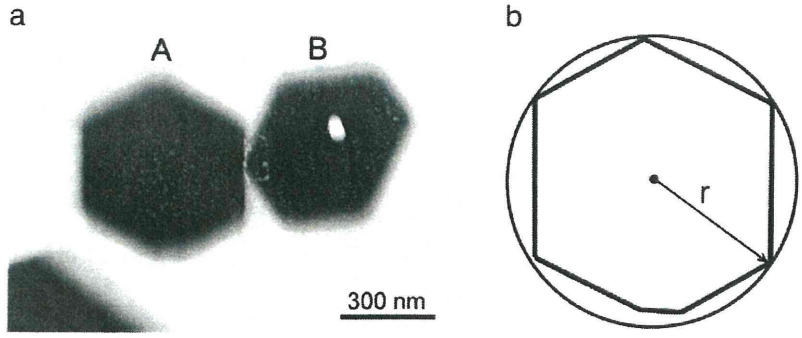

Fig. 4. (a) Magnified TEM image for cross-sections A and B of Fig. 3 (a). (b) Circumcircle defined for cross-section A with a diameter of 630 nm.

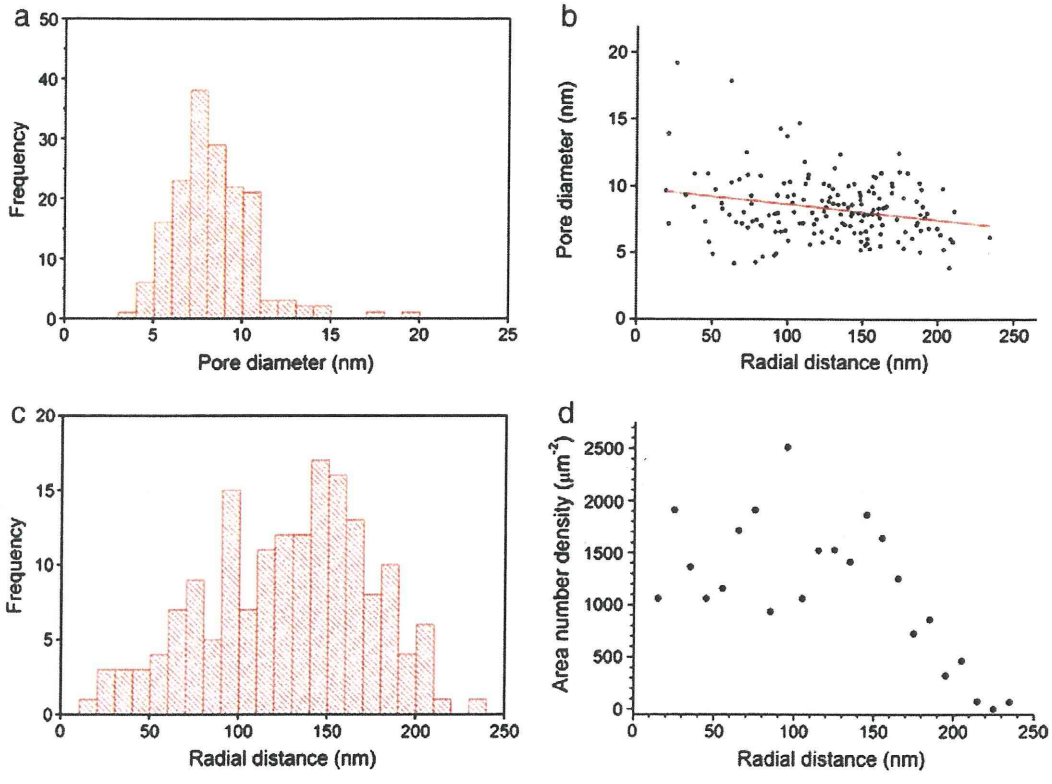

Fig. 5. (a) Pore diameter distribution of the C_{60}NW of Fig. 4 (a) A. (b) The pore diameter plotted as a function of the radial distance of pores measured from the circumcircle center (Fig. 4 (b)). (c) The radial distribution of pore number. (d) The area number density of pores plotted as a function of the radial distance of pores.

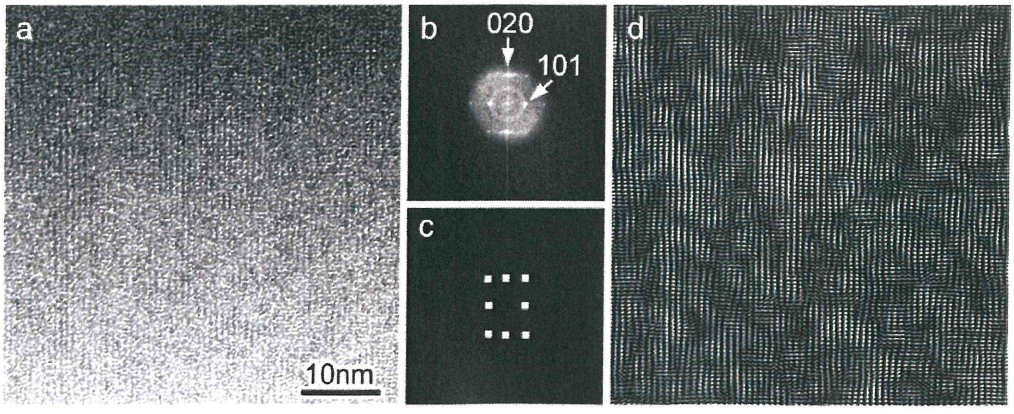

Fig. 6. (a) HRTEM image for the C_{60}NW of Fig. 4 (a) B viewed along [$\bar{1}$ 0 1] axis (bct). (b) FFT image for (a). (d) Inverse filtered FFT image for (a) constructed by using the filtered FFT pattern (c).

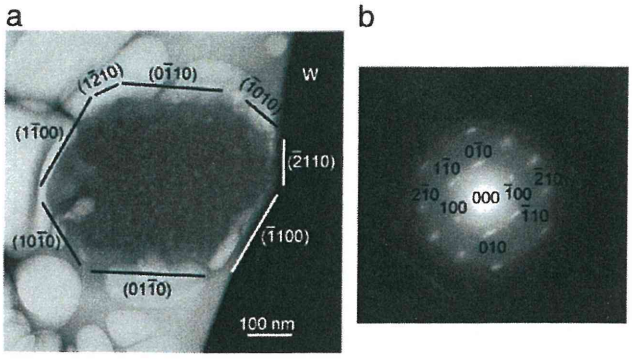

Fig. 7. (a) Cross-sectional TEM image of a C_{60}NW whose crystal faces are indexed by an hcp crystal system. (b) SAEDP for the TEM image (a) viewed along the [0 0 1] axis.

C_{60}-saturated toluene solution with the addition of a platinum derivative of C_{60}, $(\eta^2\text{-}C_{60})Pt(PPh_3)_2$, the C_{60}NWs were found to crystallize at the surface while the inner part showed a solvated soft structure [16]. This fact coincides with the present observation.

Although most of the solvent molecules may escape from the matrix upon densification at the surface, the other residual solvent molecules near the cores are conjectured to form tiny liquid bubbles and result in the formation of pores. In this study, the minimum pore size was observed to be 3.9 nm. This suggests that the critical pore diameter above which the pores can grow is about 4 nm.

Fig. 6 (a) is an HRTEM image of the cross-section shown in Fig. 4 (a) B. The fast Fourier transform (FFT) image (b) for (a) was indexed as shown in the figure, assuming a body-centered tetragonal (bct) structure with lattice constants $a = 0.99$ nm and $c = 1.5$ nm [1,3,11]. Fig. 6 (d) is an inverse FFT image formed by using the filtered FFT pattern of Fig. 6 (c). Fig. 6 (d) shows that the matrix of C_{60}NW is heavily disordered and exhibits domains with short-range ordering on the order of 5–10 nm. The intercluster distance between C_{60} molecules in the whisker is 0.99 nm. Since pristine C_{60} crystals have a face-centered cubic (fcc) structure with lattice constant $a = 1.4166$ nm [17] and the nearest neighbor distance of C_{60} molecules is 1.002 nm, the smaller intercluster distance of 0.99 nm suggests the formation of C_{60} polymer chains along the whisker growth axis. The polymerization of C_{60} molecules can occur by the irradiation of electron beams by TEM [18] which leads to the formation of bct structure from the pristine fcc structure.

Fig. 7 (a) shows a cross-sectional TEM image of a C_{60}NW with 8 vertices. The selected-area electron diffraction pattern (SAEDP) for Fig. 7 (a) is shown in Fig. 7 (b) and could be indexed by assuming a hexagonal close-packed (hcp) crystal system with lattice constant $a = 0.96$ nm. It has been known that pure C_{60} crystals can take both the hcp structure as well as the fcc structure [17,19–21]. In this example, the intercluster distance of C_{60} molecules equals 0.96 nm and is smaller than that of pristine C_{60}, suggesting electron beam polymerization. Although the length of the c-axis cannot be obtained from the SAEDP, it is calculated to be 1.6 nm by assuming a c/a ratio of 1.633 of the hcp structure [19–21]. This c-axis length is close to that of 1.5 nm of the bct system shown above.

The C_{60}NW is surrounded by the 8 crystal faces that were indexed by the Miller indices of the hexagonal system. It is found that the well-developed surfaces are the low-energy planes with low Miller indices such as $(10\bar{1}0)$, $(01\bar{1}0)$ and $(1\,\bar{1}\,0\,0)$. The smaller $(\bar{2}\,1\,1\,0)$ and $(1\,\bar{2}\,1\,0)$ crystal surfaces must have higher energy than the other crystal surfaces with lower Miller indices.

Fig. 8 (a) shows the number of vertices counted for the various observed cross-sections and expressed as a function of the diameter of C_{60}NWs. Although the number of whisker vertices ranges from 6 to 8, the most frequently observed cross-section is hexagonal as expected from the solvated hexagonal structures in solution [13,14]. No special relationship was found between the diameter and the number of vertices. However, as shown in the TEM images of B, C and D of Fig. 8 (b), the cross-section of C_{60}NWs prepared by the C_{60}-saturated benzene/IPA solution becomes irregular with decreasing diameter below 100 nm. The above result suggests that the low-energy crystal faces with low Miller indices develop with increasing whisker diameter above a critical diameter (D_c). The D_c value may be about 100 nm in the case of the benzene/IPA solvent system, since the cross-section A with a diameter of about 100 nm shows a hexagonal shape. In general, the C_{60}NWs are expected to start to grow longer when their diameter becomes greater than the critical diameters in order to develop the low-energy crystal surfaces [22]. The rounded cross-section D suggests the initial isotropic growth of C_{60}NWs.

4. Conclusions

The above research can be summarized as follows:

(1) Cross-sections of C_{60}NWs were successfully obtained through the FIB process by using samples embedded in PVA films.
(2) C_{60}NWs have a core-shell structure with dense surface thin layers and porous inner cores with mean pore diameters of about 8 nm. The number and size of the pores decrease near the surface of C_{60}NWs.
(3) The intercluster distance of the C_{60} molecules of C_{60}NWs was found to be smaller than that of pristine C_{60} crystals by TEM observations, indicating the polymerization of C_{60} molecules by electron beam irradiation.

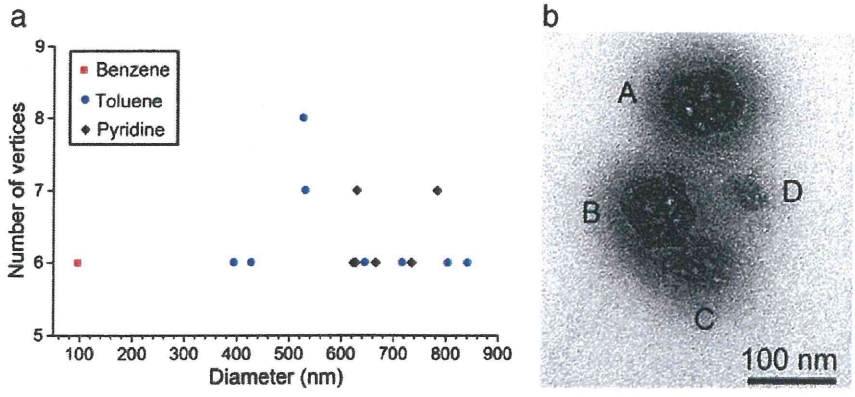

Fig. 8. (a) The number of vertices plotted as a function of diameter for the C_{60}NWs synthesized using C_{60}-saturated benzene/IPA, C_{60}-saturated toluene/IPA and C_{60}-saturated pyridine/IPA solutions. (b) Cross-sectional TEM image of the C_{60}NWs synthesized using C_{60}-saturated benzene/IPA solution.

(4) The FFT analysis for an HRTEM cross-sectional image of C_{60}NW revealed a disordered matrix composed of domains with sizes on the order of 5–10 nm.
(5) The most frequently observed cross-section of C_{60}NWs was hexagonal. A C_{60}NW was observed to be surrounded by crystal surfaces with low Miller indices of the hexagonal crystal system. It is suggested that C_{60}NWs grow longer above a critical diameter (D_c) by developing low-energy crystal surfaces.
(6) The cross-sections of C_{60}NWs became irregular and rounded with decreasing whisker diameter, suggesting the isotropic growth of C_{60}NWs with diameters smaller than D_c during their initial nucleation and growth stage.

Acknowledgements

Part of this research was supported by Health and Labour Sciences Research Grants (H21-Chemistry-Ippan-008) from the Ministry of Health, Labour and Welfare of Japan and conducted in Center for Nano Lithography & Analysis, The University of Tokyo, supported by the Ministry of Education, Culture, Sports, Science and Technology (MEXT), Japan. This work was also supported in part by World Premier International Research Center (WPI) Initiative on Materials Nanoarchitectonics, MEXT, Japan.

References

[1] K. Miyazawa, Y. Kuwasaki, K. Hamamoto, S. Nagata, A. Obayashi, M. Kuwabara, Surf. Interface Anal. 35 (2003) 117.
[2] M.P. Larsson, J. Kjelstrup-Hansen, S. Lucyszyn, ECS Trans. 2 (2007) 27.
[3] K. Saito, K. Miyazawa, T. Kizuka, Jpn. J. Appl. Phys. 48 (2009) 010217.
[4] K. Miyazawa, K. Hamamoto, S. Nagata, T. Suga, J. Mater. Res. 18 (2003) 1096.
[5] K. Miyazawa, A. Obayashi, M. Kuwabara, J. Am. Ceram. Soc. 84 (2001) 3037.
[6] T. Kizuka, K. Saito, K. Miyazawa, Diamond Relat. Mater. 17 (2008) 972.
[7] K. Asaka, R. Kato, K. Miyazawa, T. Kizuka, Appl. Phys. Lett. 89 (2006) 071912.
[8] B. Wei1, P. Kohler-Redlich, U. Bäder, B. Heiland, R. Spolenak, E. Arzt, M. Rühle, Ultramicroscopy 85 (2000) 93.
[9] K. Ogasawara, H. Kameda, Y. Matsuzaki, T. Sakurai, T. Uehara, A. Toji, N. Sakai, K. Yamaji, T. Horita, H. Yokokawa, J. Electrochem. Soc. 154 (2007) B657.
[10] M. Andrzejczuk, T. Płociński, W. Zieliński, K.J. Kurzydłowski, J. Microsc. 237 (2010) 439.
[11] K. Miyazawa, Y. Kuwasaki, A. Obayashi, M. Kuwabara, J. Mater. Res. 17 (2002) 83.
[12] K. Miyazawa, J. Minato, T. Yoshii, M. Fujino, T. Suga, J. Mater. Res. 20 (2005) 688.
[13] J. Minato, K. Miyazawa, Diamond Relat. Mater. 15 (2006) 1151.
[14] J. Minato, K. Miyazawa, Carbon 43 (2005) 2837.
[15] K. Miyazawa, J. Nanosci. Nanotechnol. 9 (2009) 41.
[16] K. Miyazawa, T. Suga, J. Mater. Res. 19 (2004) 2410.
[17] D. McCready, M. Alnajjar, Powder Diffraction File No. 44-558, International Centre for Diffraction Data, Newton Square, PA, (1994).
[18] M. Nakaya, T. Nakayama, M. Aono, Thin Solid Films 464–465 (2004) 327.
[19] W. Krätschmer, L.D. Lamb, K. Fostiropoulos, D.R. Huffman, Nature 347 (1990) 354.
[20] D.L. Dorset, J. Phys. Chem. 99 (1995) 16748.
[21] J.L. de Boer, S. van Smaalen, V. Petricek, M. Dusek, M.A. Verheijen, G. Meijer, Chem. Phys. Lett. 219 (1994) 469.
[22] K. Miyazawa, K. Hotta, J. Cryst. Growth 312 (2010) 2764.

Dispersion of carbon nanotubes and fullerene nanowhiskers by the liquid-jet cavitation method

K. Miyazawa[1]*, T.Tokumitsu[2], J.Fujii[3], R.Kato[1], S.Nudejima[1], K.Hotta[1], K.Ide[1] and T.Kizuka[3]

[1] National Institute for Materials Science (NIMS), Fullerene Engineering Group, 1-1, Namiki, Tsukuba, 305-0044 (Japan)
[2] Institute of Industrial Science, The University of Tokyo, 4-6-1 Komaba Meguro-ku, Tokyo, 153-8505 (Japan)
[3] Institute of Materials Science, University of Tsukuba, Tsukuba, 305-8573(Japan)

* *Corresponding author. E-mail : miyazawa.kunichi@nims.go.jp*

Abstract. A few papers suggesting the carcinogenicity of carbon nanotubes (CNTs) have been published recently. However, the CNTs are in general agglomerated and not always suited for their assessment of biological impact. In the present study, the liquid-jet cavitation method is examined for the dispersion of MWCNTs. It is shown that the liquid-jet cavitation method is useful to prepare isolated and well-dispersed MWCNTs. Further, it is also shown that the liquid-jet cavitation method is efficiently used to pulverize fullerene nanowhiskers into short and uniform pieces.

1. Introduction

Takagi et al. recently published a paper reporting that MWCNTs induce mesothelioma in P53 heterozygous mice [1]. Further, Poland et al. reported that exposing the mesothelial lining of the body cavity of mice to long multiwalled carbon nanotubes results in asbestos-like, length dependent, pathogenic behavior [2]. Although the above papers highlight the hazardous aspect of MWCNTs, no sufficient detailed structural characterizations for the used MWCNTs are shown. Though the MWCNTs might induce cancer as described in the above papers, it will be illogical to connect directly the carcinogenicity and MWCNTs unless well-characterized, isolated and finely dispersed MWCNTs are used for the carcinogenicity evaluation. It is considered that the agglomerated MWCNTs do not reflect the biological influence of monodispersed MWCNTs. On the other hand, the liquid-jet cavitation method is known to be a powerful technique to pulverize various materials [3]. Hence, the purpose of this paper is to investigate whether the liquid-jet cavitation method is effectively used for the pulverization and dispersion of MWCNTs. The method is also applied for the C_{60} fullerene nanowhiskers that are composed of C_{60} molecules that are connected via weak van der Waals bonding forces. This result is also shown and compared with the result of MWCNTs.

2. Experimental Methods

The MWCNTs (MWNT-7, Lot. 061220-02, Nano Carbon Technologies Co., Ltd, Japan) similar to those in the paper [1] were used in this experiment. The thermal stability of the as-received sample was examined by use of TG-DTA. The dispersed morphology of MWCNTs by the liquid-jet cavitation method using ethanol was observed by transmission electron microscopy (JEOL JEM-4010, LEO 922 Omega). Raman spectroscopy (JASCO, NRS-3100) was also used to investigate the structure of MWCNTs. The impurity iron contained in the as-received MWCNTs was measured by the atomic absorption spectrometry (AAS) and ICP - Atomic Emission Spectrometry (ICP-AES).

Short C_{60} nanowhiskers were synthesized by use of a C_{60}-saturated toluene and isopropyl alcohol [4]. These C_{60}NWs were pulverized by the liquid-jet cavitation method in the same condition with the MWCNTs.

3. Results and Discussion

The impurity iron contained in the as-received MWCNTs was measured to be 3600 ppm which is very close to 3500 ppm of MITSUI MWCNT-7 (Lot No.060125-01k) shown in ref. 1. A Raman spectroscopy profile of the as-received MWCNTs showed a high intensity of G band, suggesting that the MWCNTs are composed of well-

developed graphitic layers. The thermal decomposition temperature of the MWCNTs in air was measured to be 744 °C. This high temperature also indicates that the MWCNTs are composed of well-developed graphitic layers as suggested above.

A typical TEM image of the MWCNTs dispersed by use of an normal ultrasonic bath is shown in Figure 1. However, as shown in Figure 2, granular carbon particles composed of well-developed graphitic layers were also frequently observed among the MWCNTs. This example shows that the sample of MWCNTs contain impurity carbons that cannot be distinguished only by the Raman spectroscopy. The dispersion method using the ultrasonic bath was not successful to prepare isolated MWCNTs owing to many nodes that combine the MWCNTs as shown in Figure 3. However, the well-isolated MWCNTs were successfully obtained by use of the luquid-jet cavitation method as shown in Figure 4. The length and diameter distribution of the pulverized MWCNTs are shown in Figure 5. The length of MWCNTs ranges from ~ 1 μm to ~13 μm, while their diameter ranges from ~ 30 nm to ~ 350 nm.

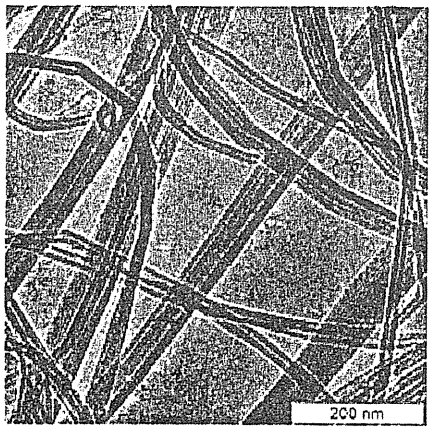

Figure 1 : TEM image of MWCNTs dispersed by use of an ultrasonic bath.

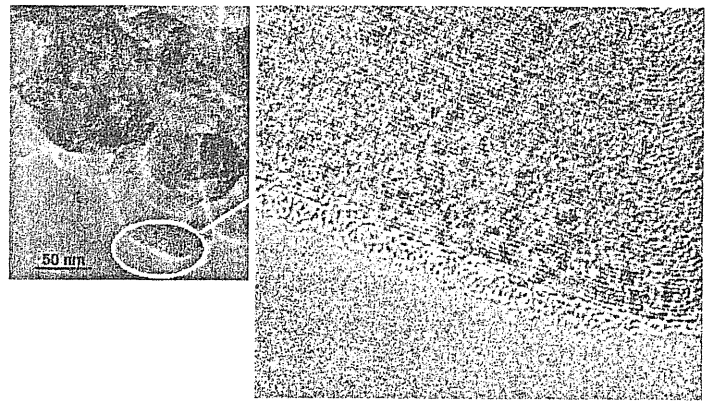

Figure 2 : HRTEM images for a part of the MWCNTs' sample.

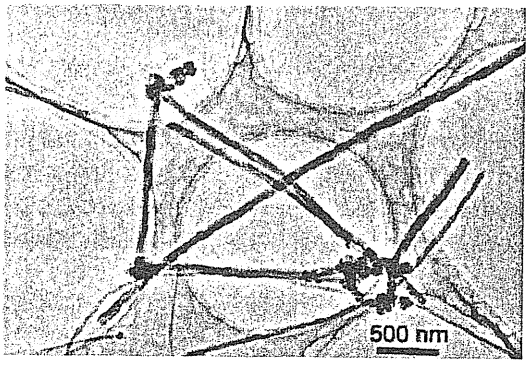

Figure 3 : TEM image of the nodes combining the MWCNTs.

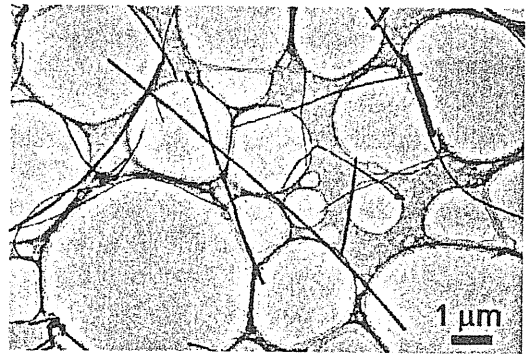

Figure 4 : TEM image of the MWCNTs dispersed by the liquid-jet cavitation method.

Figure 6 (a) shows a typical image of MWCNT with a closed end. On the other hand, Figure 6 (b) shows an example of MWCNT which was fractured by the liquid-jet cavitation method and exhibits a morphology of open end with the stepped structure, reflecting the stacked graphene layers. This image suggests that the liquid-

jet cavitation method can be effectively used to prepare such open-ended structure which will be useful for the application of field emission tips, for example.

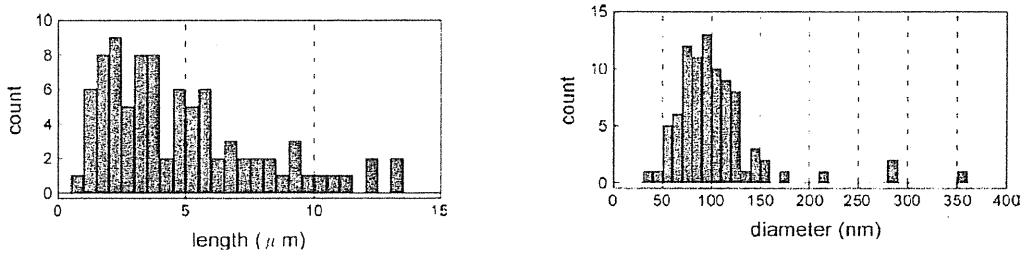

(a) (b)

Figure 5: (a) length and (b) diameter distribution of the MWCNTs pulverized by the liquid-jet cavitation method. The mean value is (a) 4.8 ± 3.1 μm in length and (b) 104 ± 49 nm in diameter, respectively.

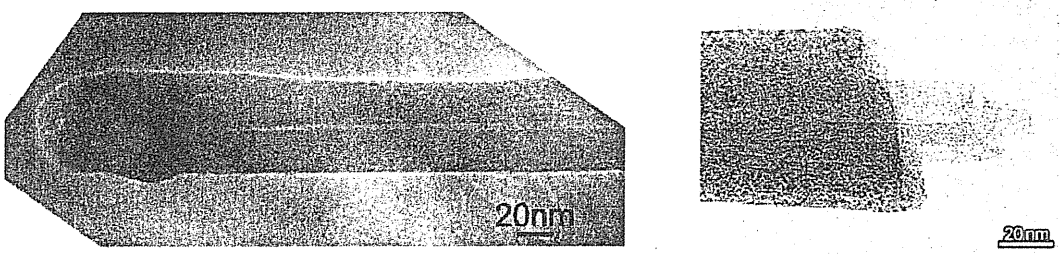

Figure 6 : TEM images of (a) MWCNT with a closed end and (b) fractured MWCNT with an open end.

Examples for the as-grown C_{60} nanowhiskers and the C_{60} nanowhiskers pulverized by the liquid-jet cavitation method which was repeatedly performed for ten cycles are shown in Figure 7. The C_{60} nanowhiskers are observed to be brittlely fractured. However, it is to be noticed that the fractured C_{60} nanowhiskers exhibit more uniformity in the length comparing with the as-grown C_{60} nanowhiskers and the above pulverized MWCNTs. As shown in Figure 8, the length of C_{60} nanowhiskers pulverized by the liquid-jet cavitation method is found to decrease with increasing the cycle number of pulverization. The standard deviation of length is also shown to decreases. This result shows that the liquid-jet cavitation method is very efficiently used in preparing the short and uniform pieces of C_{60} nanowhiskers. It is noted that the as-grown sample of C_{60} nanowhiskers have the similar length distribution with the MWCNTs of Figure 5(a).

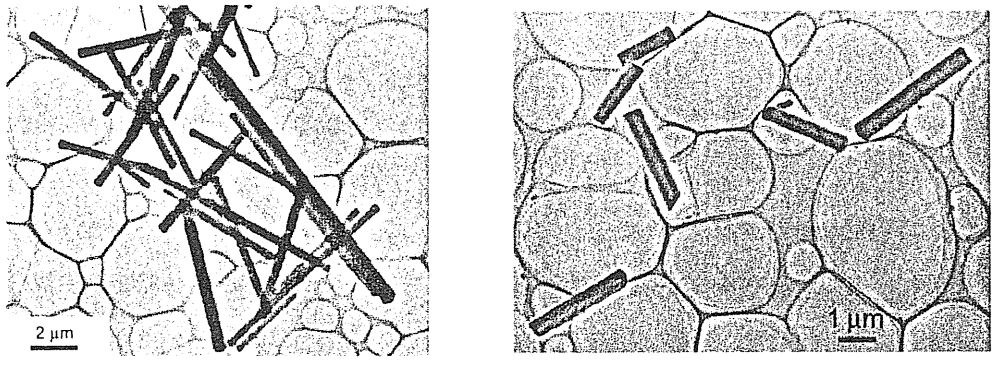

(a) (b)

Figure 7 : TEM images of (a) the as-grown C_{60} nanowhiskers and (b) the C_{60} nanowhiskers pulverized by the liquid-jet cavitation method repeated for ten cycles.

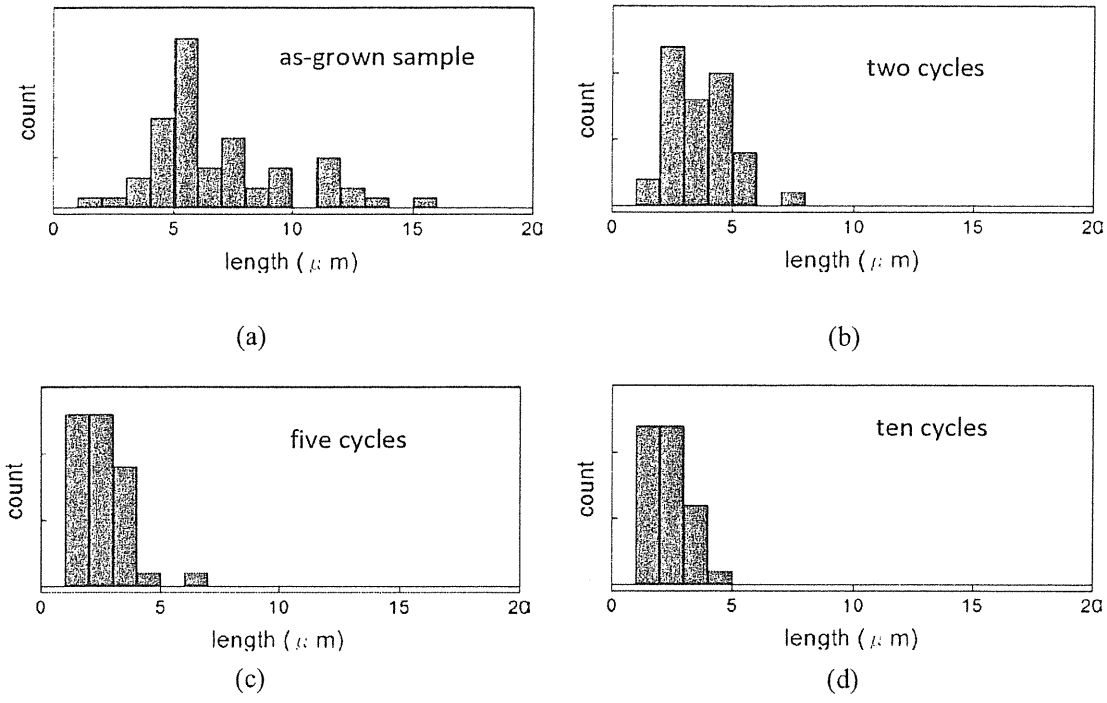

Figure 8 : Change of the length of C_{60} nanowhiskers as a function of the number of cycles in the liquid-jet cavitation method. The mean length of C_{60} nanowhiskers is (a) 6.9 ± 3.0 μm (as-grown), (b) 3.6 ± 1.3 μm (pulverized), (c) 2.6 ± 1.0 μm (pulverized) and (d) 2.4 ± 0.7 μm (pulverized) , respectively.

4. Conclusion

It has been proved that the liquid-jet cavitation method is very efficient in preparing the isolated MWCNTs for their biological impact assessment. The nodes that bind the MWCNTs can be removed by the liquid-jet cavitation method. It has been also shown that this method is also applicable to pulverize the C_{60} nanowhiskers into short and uniform pieces. As shown in the above, the liquid-jet cavitation method will be widely used in the field of biological impact assessment of dispersed nanomaterials including carbon nanotubes and fullerene nanowhiskers.

Acknowledgement

The authors are grateful to Dr. Shuji Tsuruoka (Mitsui & Co.,Ltd.) for the supply of MWCNTs and Mr.Hideo Tsunakawa (The University of Tokyo) for the use of HRTEM. .

References

[1] A.Takagi, A.Hirose, T. Nishimura, N.Fukumori, A.Ogata, N.Ohashi, S. Kitajima and J.Kanno, J. Toxicol. Sci. **33**(2008)105-116.

[2] C. A. Poland, R. Duffin, I.Kinloch, A.Maynard, W.A.H. Wallace, A.Seaton, V.Stones, S.Brown, W.Macnee and K.Donaldson, Nature Nanotech. **3**(2008)423-428.

[3] K.Tokumitsu, Materials Science Forum **360-362** (2001)397-402.

[4] K.Hotta and K.Miyazawa, NANO **3**(2008) 355-359.

技術解説

フラーレンナノファイバの合成と成長機構

物質・材料研究機構
宮澤　薫一

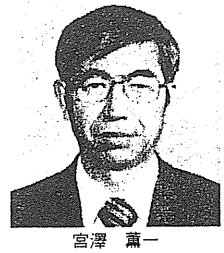
宮澤　薫一

アブストラクト：

フラーレンナノファイバとは，フラーレン誘導体や原子内包フラーレンを含むあらゆるフラーレン分子からなる細い繊維状物質であり，それらの直径が1 000 nm未満のものを指す．フラーレンナノファイバは，中空でないフラーレンナノウィスカと中空なフラーレンナノチューブの2種類に大別される．フラーレンナノウィスカは，通常，単結晶の構造をもっている．2001年のC_{60}ナノウィスカの発見以来，フラーレンナノファイバの研究が世界的に展開されるようになり，フラーレンナノファイバは，フラーレンナノロッドやフラーレンナノワイヤなどとも呼ばれるようになった．中でもC_{60}ナノファイバが，物性と応用において最もよく研究されている．本稿では，主としてC_{60}ナノウィスカの合成と，その成長機構について述べる．

1．はじめに

ファイバとは，文献1）によると長さに対する直径の比が3以上の粒子として定義される．ファイバのアスペクト比は，機械的性質に影響を及ぼす複合材料フィラーにとって重要なパラメータである．一方，ここで紹介するフラーレンナノファイバ（fullerene nanofiber）とは，C_{60}，C_{70}，金属内包フラーレン，フラーレン誘導体などのあらゆるフラーレン分子からなる細いファイバであり，それらの直径は1 000 nm未満である[2]．さまざまなフラーレンナノファイバの中でも，C_{60}ナノファイバが，構造，機械的性質，熱的性質，化学的性質において，また，電界効果トランジスタ（FET），太陽電池，マイクロ燃料電池などの応用において，今日まで最もよく研究されている[2) 3)]．

フラーレンナノファイバは，中空なもの，中空でないものの二つの形状が可能である．中空でないものは，フラーレンナノウィスカ（fullerene nanowhisker）といい，単結晶の構造をもっている．中空なフラーレンナノファイバは，フラーレンナノチューブと呼ばれている．

2001年のC_{60}ナノウィスカの発見以来[4]，フラーレンナノファイバの研究が世界的に拡大しつつあり，最近では，フラーレンナノファイバを，フラーレンナノロッド（fullerene nanorod），フラーレンナノワイヤ（fullerene nanowire），フラーレンナノベルト（fullerene nanobelt）と呼ぶ論文も出版されている[2]．

ここでは，主としてC_{60}ナノウィスカの合成と，その成長機構について得られた知見を述べる．

2．液 - 液界面析出法

C_{60}ナノウィスカが，2002年に液 - 液界面析出法（液 - 液界面法，液 - 液法，liquid-liquid interfacial precipitation method: LLIP法）によって初めて合成された[5]．近年，液 - 液法は著しく発展し，フラーレンナノファイバだけでなく，フラーレンナノシート（fullerene nanosheet）の合成も可能とした[6) 7)]．液 - 液法は，フラーレンナノファイバやフラーレンナノシートを，大気中で合成することができること，多様な元素を添加することができること，複数のフラーレン分子からなる複合組成

宮澤　薫一（Kunichi Miyazawa）
1979年　東京大学農学部林学科卒業
1981年　東京大学教養学部基礎科学科卒業
1985年　東京大学生産技術研究所文部技官
1986年　東京大学工学部精密機械工学科助手
1987年　工学博士
1989年　東京大学工学部金属材料学科講師
2002年　物質・材料研究機構主幹研究員
現　在　物質・材料研究機構フラーレン工学グループリーダー
■主として行っている業務・研究
フラーレンナノ物質の合成と応用．
■勤務先
物質・材料研究機構ナノテクノロジー基盤萌芽ラボ
〒305-0044　茨城県つくば市並木1-1

のものが合成できること，それらの大きさや形状を，温度，溶媒，濃度，光環境を変化させて変えることができることなどの優れた特長をもっている．また，合成に用いる道具は，ガラス器具と冷蔵庫があれば可能であり，特殊な装置を用いなくてよいこともメリットである．

液 - 液法を用いると多様な形状のフラーレンナノ物質を合成することができる．例えば，C_{60} を飽和させたトルエン溶液とイソプロピルアルコールの組合せによって C_{60} ナノウィスカを合成することができる[2) 5)]．一方，C_{70} 分子からなる中空な単結晶ナノファイバである C_{70} ナノチューブは，C_{70} 飽和ピリジン溶液とイソプロピルアルコールの組合せによって合成することができる[8)]．また，C_{60} ナノシートは，C_{60} を飽和させた四塩化炭素とイソプロピルアルコールの組合せや，フェロセンを添加した C_{60} 飽和トルエン溶液とイソプロピルアルコールの組合せにより合成することができる[6) 7)]．

以上のように，液 - 液法は，フラーレンの良溶媒（トルエン，四塩化炭素，ベンゼンほか）と貧溶媒（イソプロピルアルコール，イソブチルアルコール[9)] ほか）の組合せを用いている．フラーレンの良溶媒飽和溶液と貧溶媒がつくる液 - 液界面においては，良溶媒と貧溶媒とが混和することによって，フラーレンの過飽和状態*が実現し，フラーレンの結晶核が形成され，それらの結晶核からフラーレンナノファイバが成長する．

図 1　C_{60} 飽和トルエン溶液にイソプロピルアルコールを重層して生じた液 - 液界面で，C_{60} 結晶核の析出が生じている様子

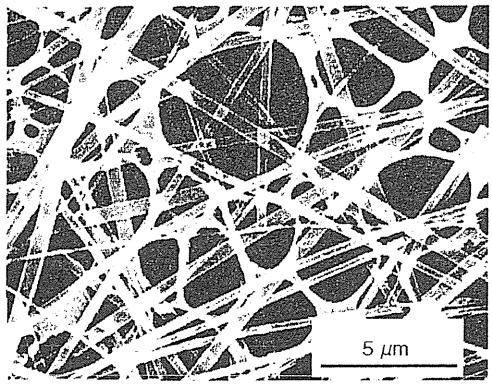

図 2　C_{60} ナノウィスカの SEM 像

3. C_{60} ナノウィスカの成長制御

液 - 液界面析出法による C_{60} ナノウィスカの合成は，図 1 に示すように，C_{60} 飽和トルエン溶液をガラスビンに入れ，イソプロピルアルコールを重層し，液 - 液界面にて C_{60} 結晶核を生成させることから始まる．このガラスビンを，室温以下の温度に設定した恒温槽に置くことにより自己組織的に C_{60} ナノウィスカが成長する．図 2 に，長く成長した C_{60} ナノウィスカの走査電子顕微鏡（SEM）像を示す．

液 - 液界面を形成した後で，ガラスビンを意図的に振って一様な懸濁液をつくり恒温槽にセットすることで，短いが均一な長さの C_{60} ナノウィスカを合成することも可能である．フラーレンナノファイバの高度利用のためには，アスペクト比や直径を自由に制御する技術を確立することが必要である．例えば，フラーレンナノファイバを導電ファイバとして用いるときは，できるだけ長く成長させることが必要であり，太陽電池に使用する場合は，短いフラーレンナノファイバが必要となる[10)]．

橘らによって，C_{60} ナノウィスカの成長が，C_{60} 飽和トルエン溶液とイソプロピルアルコールの系において，光によって促進されることが発見された[11)]．また，C_{60} 飽和ピリジン溶液とイソプロピルアルコールの系においては，C_{60} ナノチューブの収量が，液 - 液界面を形成する前の C_{60} 飽和ピリジン溶液に照射される光の波長に依存して変わることが明らかになった．この理由は不明であるが，光励起一重項 C_{60} から遷移して生じる三重項 C_{60} による波長 740 nm 付近の光吸収と関係していると考察されている[12) 13)]．

一般に，フラーレンナノファイバの成長が光の波長に依存して変化することは，ガラスビンの色を変えた場合にも，その収量の変化として観察されることが期待される．このことを確かめるために，褐色ガラスビンと透明ガラスビンの二つを用いた実験を，C_{60} のトルエン溶液とイソプロピルアルコールの系で行うことを

＊ 過飽和状態：溶媒中に溶質が溶けている均一な混合液を溶液と呼ぶ．溶解度とは，平衡状態で溶媒中に溶けている溶質の飽和濃度のことである．溶液が過飽和状態になると，結晶が析出し成長する．過飽和溶液の濃度を x，同じ温度での飽和濃度を y とすると，過飽和度は，$(x-y)$ により定義される．

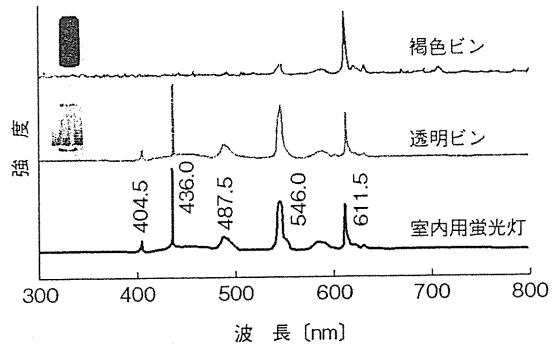

図3 褐色ビンと透明ビンを透過する光（室内蛍光灯）のスペクトル

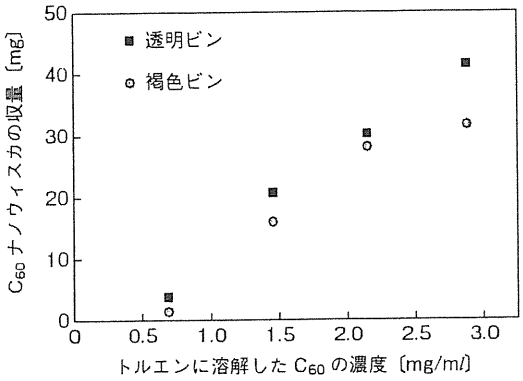

図4 褐色ガラスビンと透明ガラスビンにおける C_{60} ナノウィスカの収量の比較

試みた．図3は，室内蛍光灯を光源とした場合の褐色ビンと透明ビンを透過する光のスペクトルを比較したものである．褐色ビンは，600 nm 以下の波長の光を効果的にカットしており，特に，約 500 nm 以下の波長の光を完全にカットしている．図4は，5℃の液温において，褐色ビンと透明ビンのそれぞれにおける C_{60} ナノウィスカの収量を，さまざまな濃度の C_{60} トルエン溶液について示したものである．C_{60} トルエン溶液とイソプロピルアルコールを等容（各 20 ml）とした場合の結果である．

C_{60} ナノウィスカの収量が，褐色ビンに比べて透明ビンのほうが高くなっているように，ガラスビンの色に応じて，収量が変化することがわかった．今後は，C_{60} ナノウィスカの収量が，光量と光の波長の関数として，どのように変化するのかを調べることが必要である．

図5に示すように，C_{60} ナノウィスカの直径にも違いが見られており，透明ビンでは，平均直径が 382 ± 121 nm，褐色ビンでは，平均直径が 441 ± 185 nm の C_{60} ナノウィスカが合成されている．透明ビンで合成された C_{60} ナノウィスカのほうが，褐色ビンの場合よりも平均直径がより小さくなっているが，これは，光照射によって，より小さな核からの成長が促進されること

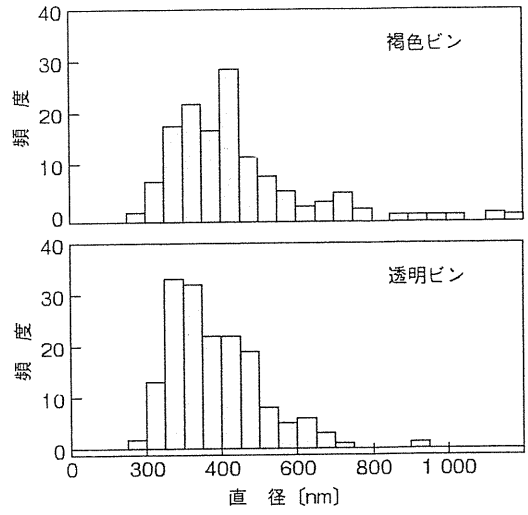

図5 透明ガラスビンと褐色ガラスビンにおける C_{60} ナノウィスカの直径の頻度分布

を示している．このことから，細い C_{60} ナノウィスカを得るためには，より短い波長の光をより多く照射することが効果的であると推察される．

上記のように，C_{60} ナノウィスカの成長には光の波長のほかに，光量が寄与していると推察されるが，温度も重要な成長因子であり，液温を高くすると成長が促進されることが明らかになっている．C_{60} 飽和トルエン溶液とイソプロピルアルコールの系における C_{60} ナノウィスカの成長速度の温度依存性の測定から，C_{60} ナノウィスカの成長の活性化エネルギーが 52.8 kJ/mol と求められた[14]．この値は，文献 15）で報告されている溶液中（トルエン：アセトニトリル＝4：1，0.1 M $(n\text{-}Bu_4N)PF_6$ 添加）における C_{60} の拡散の活性化エネルギー 13.1 kJ/mol に比べて非常に大きく，表面集積過程において，C_{60} 分子からの溶媒分子の脱離エネルギー（脱溶媒和エネルギー）が大きいことを示している．C_{60} 分子は溶媒和結晶をつくりやすく，C_{60} ナノウィスカは溶液中では六方晶であり，大気中では溶媒を失って面心立方晶に変化することが知られている[2]．

さらに，C_{60} 飽和トルエン - イソプロピルアルコールの系において，C_{60} ナノウィスカの成長が，イソプロピルアルコールに添加された少量の水によって大きく影響されることがわかった．図6は，イソプロピルアルコールに水を添加した場合において，液 - 液界面を形成後，24 時間経過後の C_{60} ナノウィスカの生成の様子を示す．

図7は，図6の各ガラスビンから採取された C_{60} ナノウィスカのアスペクト比が，イソプロピルアルコール中に含まれる水の量が増加するにつれて，増加することを示している．つまり，図7は，C_{60} ナノウィスカの成長に水が触媒として作用していることを示してい

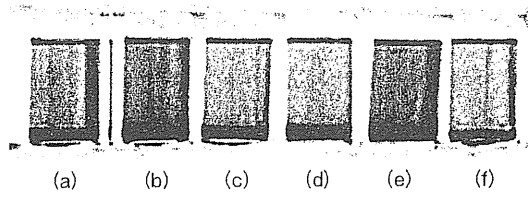

図6 C_{60} 飽和トルエン溶液（4 ml）と水を添加したイソプロピルアルコール（4 ml）の系において，液-液界面形成後24時間後の C_{60} ナノウィスカの生成（沈殿）の様子を示す．
水のイソプロピルアルコールへの添加量（質量%）は，(a) 0%，(b) 0.4%，(c) 0.6%，(d) 0.9%，(e) 1.3%，(f) 2.5%，合成温度は20℃である

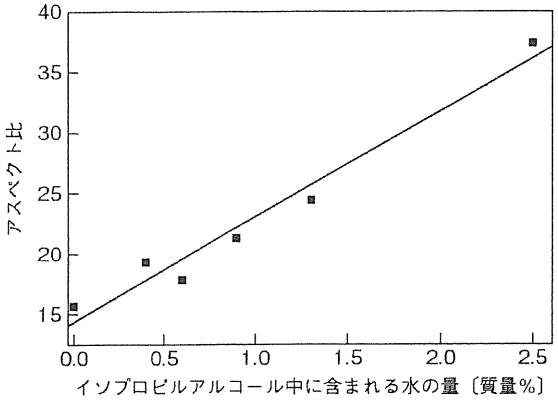

図7 C_{60} 飽和トルエン（4 ml）-イソプロピルアルコール（4 ml）の系においての，イソプロピルアルコールに添加された水分量と C_{60} ナノウィスカのアスペクト比の関係．合成温度20℃

る．水が，アルコール分子のつくるクラスタの構造を大きく変化させることが知られていることを考慮すると[16]，水の添加がイソプロピルアルコール分子のクラスタの構造を変化させて成長機構を変えることや，水が脱溶媒和エネルギーを低下させる働きをすることが考えられる．

水の添加による C_{60} ナノウィスカ側面の表面-溶媒界面エネルギーの低下や溶液中におけるプロトン濃度の変化も，成長に影響する因子として検討すべき課題である．以上の結果は，環境中の水分も C_{60} ナノファイバの成長に影響を与えることを示唆している．

水だけではなく，C_{60} 飽和トルエン溶液とイソプロピルアルコールの量比によっても C_{60} ナノウィスカの成長が大きく変化することがわかった．C_{60} 飽和トルエン溶液とイソプロピルアルコールの量比（体積比）を，1：9～9：1の間で変化させたところ，1：1組成において C_{60} ナノウィスカが最も高い収率で得られること，また，イソプロピルアルコールが少なすぎると，塊状の C_{60} 結晶が生じて，C_{60} ナノウィスカが合成されないことがわかった．これらのことから，C_{60} ナノウィスカの異方性成長においては，イソプロピルアルコールが

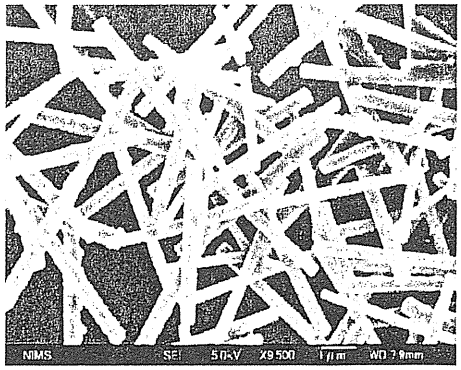

図8 C_{60} 飽和トルエン溶液とイソプロピルアルコールの体積比を1：1としたときに合成された C_{60} ナノウィスカの様子（SEM像）．合成温度20℃

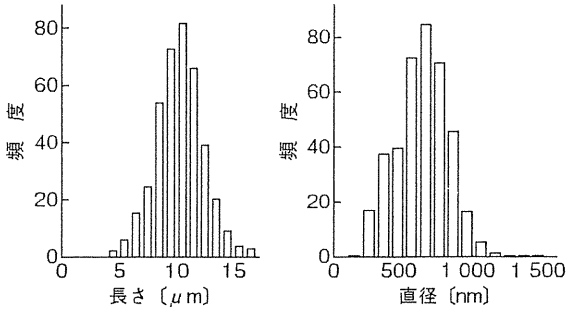

図9 C_{60} 飽和トルエン溶液とイソプロピルアルコールの系で合成された C_{60} ナノウィスカの直径と長さの測定例

C_{60} 結晶核の過飽和析出現象を支配するだけではなく，界面エネルギーをもコントロールする役目をも担っていることがわかる．

図8に，C_{60} 飽和トルエン溶液とイソプロピルアルコールの体積比を1：1としたときに合成された C_{60} ナノウィスカの様子を示す．これは，液-液界面を形成してから24時間経過後の C_{60} ナノウィスカの例である．ほぼ均一な長さの C_{60} ナノウィスカが合成されている．図9に，C_{60} 飽和トルエン溶液とイソプロピルアルコールの系で合成された C_{60} ナノウィスカの直径と長さの測定例を示す．この例では，C_{60} ナノウィスカの平均長さが10.3 ± 2.1 μm，平均直径が632 ± 194 nmとなっており，均一な長さの短いフラーレンナノウィスカが合成されている．

図10には，平均長さが1.7 ± 0.8 μm，平均直径が323 ± 103 nmの C_{60} ナノウィスカの合成例を示す．このような短いフラーレンナノウィスカは，フラーレンナノウィスカを用いた厚膜太陽電池の作製において有用であろう[10]．

C_{60} ナノウィスカの長さと直径に関して，さらに，詳細な研究を進めた．その結果を図11に示す．図11は，C_{60} 飽和トルエン溶液とイソプロピルアルコールの量比（体積比）を変えた場合の C_{60} ナノウィスカの直径と長

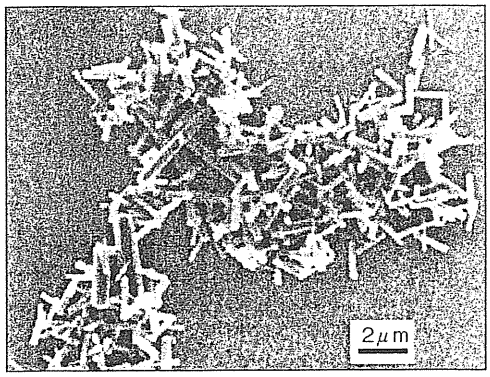

図 10　短い C_{60} ナノウィスカの合成例（SEM 像）

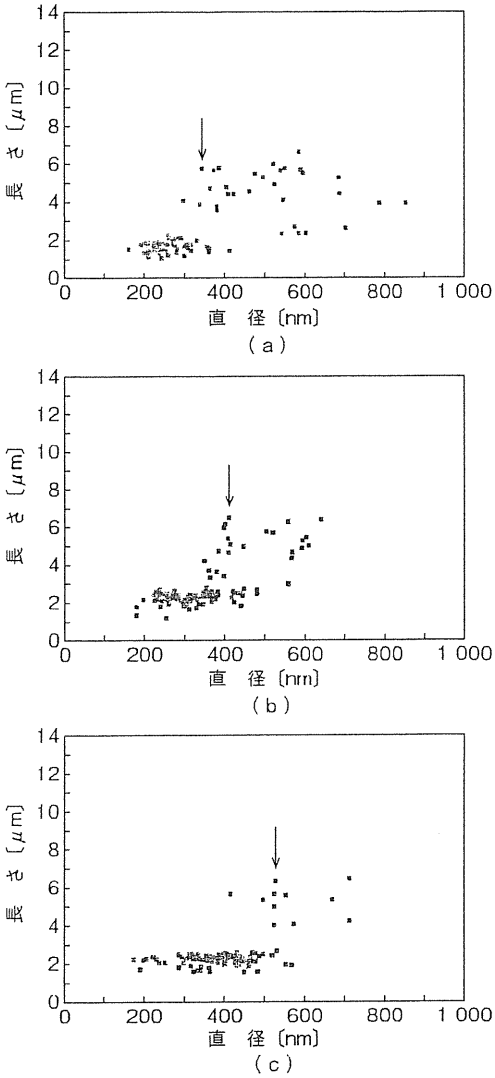

図 11　C_{60} 飽和トルエン溶液とイソプロピルアルコールの系で合成された C_{60} ナノウィスカの直径と長さの関係．
C_{60} 飽和トルエンとイソプロピルアルコールの量比（体積比）は，(a) 1：7，(b) 1：5，(c) 1：3 である

さの関係を示している．矢印で示した場所から，突然，直径と長さの分布が変化していることがわかる．

矢印で示した直径を臨界直径（d_c）と定義すると，d_c は，(a) 約 340 nm，(b) 約 400 nm，(c) 約 530 nm と

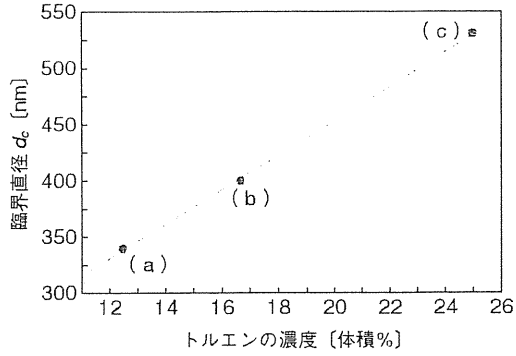

図 12　混合溶媒中におけるトルエンの濃度と臨界直径との関係

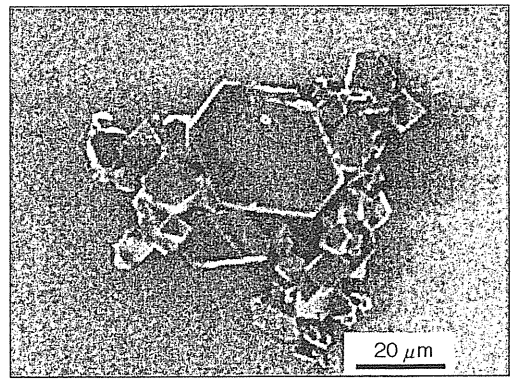

図13　C_{60} 飽和トルエン溶液：イソプロピルアルコール =3:1（体積比）の系で生じたバルク状 C_{60} 結晶

なる．イソプロピルアルコールの添加量が小さくなるほど，すなわちトルエンの濃度が高くなるほど，d_c が大きくなることがわかる（図 12）．臨界直径とトルエン濃度は直線関係にある．このことは，過飽和な状態をもたらす貧溶媒の添加量が少なくなると等方的に成長すること（図 13 に例示），逆に，過飽和度が高くなると等方的成長から，異方性成長に移行することを示している．

C_{60} ナノウィスカの長さは，その直径 d が d_c に到達するまで大きくならないことは，$d < d_c$ においては C_{60} 結晶核が等方的に成長し，$d > d_c$ においては C_{60} 結晶核が異方的に成長すること，すなわちファイバ状に成長することを示している．この異方性成長は，C_{60} ナノウィスカと溶液との間の全界面エネルギーが小さくなるように生じること，すなわち成長軸に平行な晶帯軸に属する結晶面が発達するように成長が進んで，ファイバ状に成長すると考えられる．しかし，溶媒の組合せによっては，シート状に成長したほうが安定な場合があり，表面とバルクの両方に関するエネルギーを考察しないと，なぜ，異方性成長が生じるのかについて明瞭な答えを得ることは難しく，今後の課題である．

4. まとめ

液-液界面析出法により，短い針状結晶状，長いファイバ状，平面シート状などの多様なフラーレンナノ物質を合成することができる．フラーレンナノウィスカとフラーレンナノチューブの総称であるフラーレンナノファイバの結晶成長メカニズムが，速度論的方法によってしだいに明らかになりつつある．筆者らは，温度，光，濃度のほかに，新たに，C_{60} ナノウィスカの成長に及ぼす水の触媒効果と，C_{60} 結晶核生成直後の等方性成長からファイバ状への異方性成長に変化する際の臨界直径の存在を発見した．しかも，臨界直径は，混合溶媒中における C_{60} の溶媒濃度と直線的な関係があることも明らかになった．

謝　辞

本研究を遂行するに当たり，堀田賀洋子氏（NIMS研究員）と藤井 純氏（筑波大学）のご協力をいただきました．篤く御礼申し上げます．

参　考　文　献

1) Nanoscience and nanotechnologies: Opportunities and uncertainties, The Royal Society & The Royal Academy of Engineering, p. 37 (2009)
2) K. Miyazawa : Synthesis and properties of fullerene nanowhiskers and fullerene nanotubes, J. Nanosci. Nanotechnol., **9**, p. 41 (2009)
3) Q. Wang, Y. Zhang, K. Miyazawa, R. Kato, K. Hotta and T. Wakahara: Improved fullerene nanofiber electrodes used in direct methanol fuel cells, J. Physics: Conference Series, **159**, 012023 (2009)
4) K.Miyazawa, A. Obayashi and M. Kuwabara: C_{60} nanowhiskers in a mixture of lead zirconate titanate sol-C_{60} toluene solution, J. Am. Ceram. Soc., **84**, p. 3037 (2001)
5) K. Miyazawa, Y. Kuwasaki, A. Obayashi and M. Kuwabara: C_{60} nanowhiskers formed by the liquid-liquid interfacial precipitation method, J. Mater. Res., **17**, p. 83 (2002)
6) M. Sathish and K. Miyazawa: Size-tunable hexagonal fullerene (C_{60}) nanosheets at liquid-liquid interface, J. Am. Chem. Soc., **129**, p. 13816 (2007)
7) T. Wakahara, M. Sathish, K. Miyazawa, C. Hu, Y. Tateyama, Y. Nemoto, T. Sasaki and O. Ito: Preparation and optical properties of Fullerene/ferrocene hybrid hexagonal nanosheets and large-scale production of fullerene hexagonal nanosheets, J. Am. Chem. Soc., **131**, p.9940 (2009)
8) K. Miyazawa, J. Minato, T. Yoshii, M. Fujino and T. Suga: Structural characterization of the fullerene nanotubes prepared by the liquid-liquid interfacial precipitation method, J. Mater. Res., **20**, p. 688 (2005)
9) K. Miyazawa, J. Minato, T. Yoshii and T. Suga: Characterization of fullerene nanotubes prepared by the liquid-liquid interfacial precipitation method, Sci. Technol. Adv. Mater., **6**, p. 388 (2005)
10) P. R. Somani, S. P. Somani and M. Umeno: Toward organic thick film solar cells: Three dimensional bulk heterojunction organic thick film solar cell using fullerene single crystal nanorods, Appl. Phys. Lett., **91**, 173503 (2007)
11) M. Tachibana, K. Kobayashi, T. Uchida, K. Kojima, M. Tanimura and K. Miyazawa: Photo-assisted growth and polymerization of C_{60} 'nano' whiskers, Chem. Phys. Lett., **374**, p. 279 (2003)
12) C. L. Ringor and K. Miyazawa: High yield preparation of fullerene nanowhiskers and nanotubes by the solution route, NANO, **3**, p. 329 (2008)
13) T. Akasaka, Y. Maeda, T. Wakahara, M. Okamura, M. Fujitsuka, O. Ito, K. Kobayashi, S. Nagase, M. Kako, Y. Nakadaira and E. Horn: Novel metal-free bis-silylation: C_{60}-sensitized reaction of disilirane with benzonitrile, Org. Lett., **1**, p. 1509 (1999)
14) K. Hotta and K. Miyazawa: Growth rate measurement of C_{60} fullerene nanowhiskers, NANO, **3**, p. 355 (2008)
15) M. Wei, H. Luo, N. Li, S. Zhang and L. Gan: Study of electrochemical properties of pyrrolidinofullerenes by microelectrode voltammetry, Microchem. J., **72**, p. 115 (2002)
16) J. -H. Guo, Y. Luo, A. Augustsson, S. Kashtanov, J. -E. Rubensson, D. K. Shuh, H. Agren and J. Nordgren: Molecular structure of alcohol-water mixtures, Phys. Rev. Lett., **91**, 157401 (2003)

Fullerene Nano Materials (Symposium N of IUMRS-ICA2008) IOP Publishing
Journal of Physics: Conference Series **159** (2009) 012008 doi:10.1088/1742-6596/159/1/012008

Observation of phagocytosis of fullerene nanowhiskers by PMA-treated THP-1 cells

S Nudejima[1], K Miyazawa[1], J Okuda-Shimazaki[2] and A Taniguchi[2]
[1] Advanced Nano Materials Laboratory, National Institute for Materials Science (NIMS), Tsukuba, Ibaraki, 305-0044, Japan
[2] Biomaterials Center, NIMS, Tsukuba, Ibaraki, 305-0044, Japan

E-mail: NUDEJIMA.Shinichi@nims.go.jp

Abstract. Phorbol 12-myristate 13-acetate (PMA)-treated THP-1 cells (macrophage-like cells) were exposed to the C_{60} fullerene nanowhiskers (C_{60}NWs) with an average length of about 6.0 μm and an average diameter of about 660 nm and observed with an inverted optical phase-contrast microscope for 48 h. The C_{60}NWs were well and stably dispersed onto the dishes of culture medium during the observation. The number of cells that internalised C_{60}NWs gradually increased after the exposure to C_{60}NWs. But no alteration of cellular morphology was observed compared to the control group without exposure to C_{60}NWs during this period in this pilot study.

1. Introduction

Nanomaterials possess enormous potentials to wide applications in various fields owing to their distinctive unique properties. But potential risks caused by exposure to nanomaterials have not been cleared. With the release of industrial products of nanomaterials into environment, public concerns have raised their potential side effects. Carbon nanotubes (CNTs), one of the most promising nanomaterials, may be hazardous to health and environment owing to their needle-like morphology and strong mechanical properties like asbestos. Recently, an asbestos-like pathogenic behavior associated with CNTs indicated a structure-activity relationship based on length, to which asbestos and other pathogenic fibers conform [1].

Fullerene nanowhiskers (FNWs) are composed of the fullerene molecules that are usually bonded via van der Waals forces [2]. FNWs are expected to have various application fields such as low-dimensional semiconductors, field emission tips, nanoprobes for microdevices, fiber-reinforced nanocomposites, composite elements for lubrication, and so on. But FNWs also have the needle-like morphology like asbestos. Hence, it is of great importance to evaluate the biological impacts of FNWs for their sound application in advance.

Macrophages are one of the immune system cells and defend the host against the foreign substances in a non-specific manner during the initial phase of infection. Macrophages recognize, internalise and digest them. THP-1 is a human acute monocytic leukemia cell line and THP-1 cells have been isolated by Tsuchiya et al [3]. It is well known that THP-1 cells are induced to differentiate into macrophage-like cells by the addition of PMA [4].

In this paper, the interaction of C_{60}NWs with macrophage-like cells is investigated as a pilot study for evaluating the biological impacts of C_{60}NWs by use of an inverted optical phase-contrast microscope.

2. Materials and methods

2.1. Preparation and characterization of C_{60}NWs

C_{60}NWs were prepared by the liquid-liquid interfacial precipitation method using a C_{60}-saturated toluene solution and isopropyl alcohol (Fig.1) [2]. 20 mL of isopropyl alcohol was gently added to 20 mL of C_{60}-saturated toluene solution in a glass bottle at room temperature. After manual mixing, the solution was kept at 15°C for 15 minutes and 60 mL of isopropyl alcohol was poured into the solution to stop the crystal growth. The C_{60}NWs were separated by filtration using a GFP filter (0.8 μm, Kiriyama glass, Japan) from the solvents. The characterization was carried out by measuring the length and diameter of C_{60}NWs using an optical microscope (ECLIPSE ME600, Nikon, Japan) and a scanning electron microscope (JSM-6700, JEOL, Japan). C_{60} (99.5%) was purchased from MTR (OH). Toluene (99.5%) and 2-propanol (99.7%) were purchased from Wako Pure Chemical Industries (Japan).

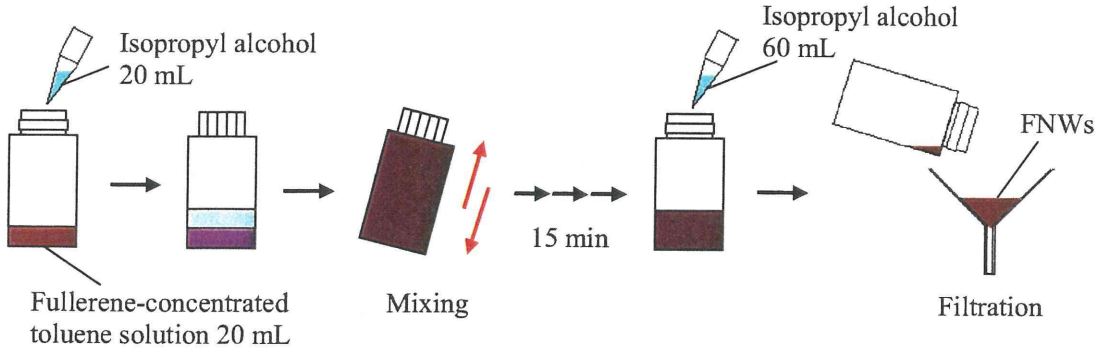

Figure 1. Preparation of C_{60}NWs

2.2. Cell culture

THP-1 cells were purchased from American Type Culture Collection (ATCC, VA). THP-1 cells were cultured in RPMI 1640 medium (Invitrogen, CA) supplemented with 10% heat inactivated fetal bovine serum (JRH Biosciences, KS), 100 units/mL penicillin and 100 μg/mL streptomycin (Nacalai Tesque, Japan)(culture solution) at 37°C in an atmosphere of 5% CO_2 and saturated humidity. Cells were subcultured every three or four days, where the number of cells in culture were maintained by centrifugation (at 1000 rpm for 3 min) and subsequent resuspension at 2 x 10^5 viable cells/mL.

2.3. Differentiation of THP-1 cells into macrophage-like cells

2 x 10^5 cells were incubated in 2 mL of culture solution on a 35 mm polystyrene culture dish (Greiner Bio-One, Germany). PMA (Wako pure chemicals, Japan) was dissolved in dimethylsulfoxide at a concentration of 1 mM and diluted by a culture solution to be 50, 500 and 5000 nM. And 40 μL of each PMA solution was added to the cellular medium to be the final concentrations of 1, 10 and 100 nM. The cells were induced to differentiate into macrophage-like cells for 1, 3, 6, 24, 48 and 72 h at 37°C in an atmosphere of 5% CO_2 and saturated humidity. To estimate the degree of differentiation, the number of suspended living cells (undifferentiated cells) was measured using 0.4% trypan blue stain (Invitrogen, CA) and the morphological changes of cells were observed by an inverted optical phase-contrast microscope (DMIL-HC, Leica Microsystems, Germany).

2.4. C_{60}NWs' exposure

C_{60}NWs were dispersed in the culture solution at a concentration of 1 mg/mL and diluted by the culture solution to be 0.1 and 0.01 mg/mL. Macrophage-like cells were exposed to 20 μL of each concentration of C_{60}NWs suspension agitated by ultrasonication to be the final concentrations of 0.1, 1

and 10 μg/mL and incubated for 1, 3, 6, 24 and 48 h at 37°C in an atmosphere of 5% CO_2 and saturated humidity. Cells were observed with the inverted optical phase-contrast microscope to evaluate the effect of C_{60}NWs on the cell morphology.

3. Results and disucussion

3.1. C_{60}NWs

3.1.1. *Characterization of C_{60}NWs*

C_{60}NWs were synthesized by the liquid-liquid interfacial precipitation method (Fig.2)[2]. The length of C_{60}NWs ranged from 1 to 17 μm approximately and the average length was about 6.0 μm (Fig.3). The diameter of C_{60}NWs ranged from 300 to 1340 nm and the average diameter was about 660 nm (Fig.4).

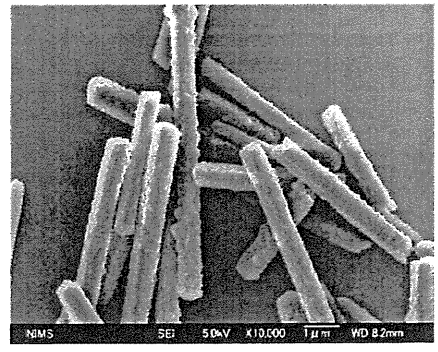

Figure 2. SEM image of C_{60}NWs.

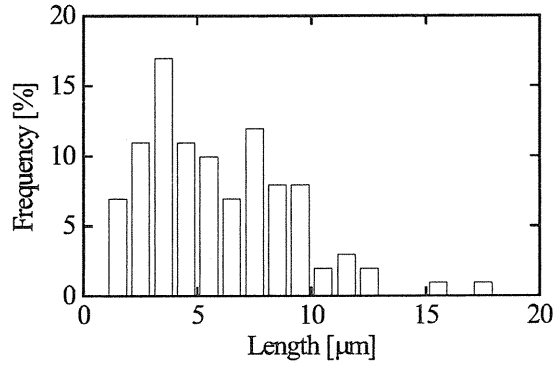

Figure 3. Histogram of C_{60}NWs' length.

3.1.2. *Dispersion of C_{60}NWs in culture*

Before exposuring cells to C_{60}NWs, the dispersion of C_{60}NWs in culture was examined visually by the inverted optical phase-contrast microscope for the same period. The suspensions of C_{60}NWs were poured into the cell-free medium by the same method as the exposure examination. The C_{60}NWs were well and stably dispersed onto the dishes of culture medium during observation (Fig.5).

3.2. Effect of PMA concentration and induction period on differentiation of THP-1 cells into macrophage-like cells

Optimal PMA concentration and induction period for the differentiation of THP-1 cells into macrophage-like cells were estimated under the condition of this study. In the case of 10 nM and 100 nM, cells adhered to the dish surface gradually (decrease of suspended cells) and about 90% of seeded cells adhered after 24 h of the PMA treatment (Fig.6). By contrast, the suspended cells grew by a factor of 5 in comparison with the seeded cells during 72 h in control culture (without PMA treatment). At the concentration of 1 nM, a few cells adhered the dish surface (data not shown), but the number of suspended cells increased about by a factor of 2 during 72 h. We observed that some of the cells showed elongation and pseudopodia formation after a few hours of the treatment by 10 nM and 100 nM (data not shown) of PMA, and most of the cells were observed to change their morphology by the PMA treatment of 24 h with the inverted optical phase-contrast microscope (Fig.7).

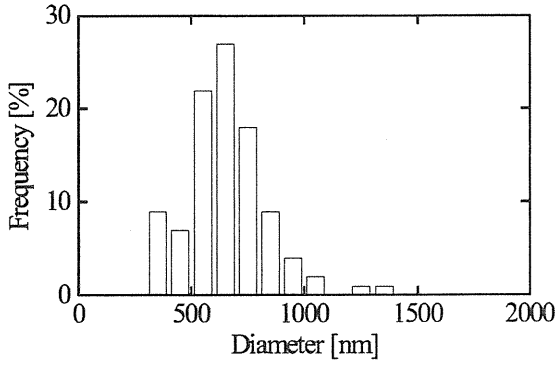

Figure 4. Histogram of C_{60}NWs' diameter.

Because no significant difference was observed in the cellular morphology and the number of adherent cells between 10 nM and 100 nM of PMA treatment, the cells differentiated by 10 nM PMA treatment for 24 h were used for the exposure experiment of C_{60}NWs.

3.3. Exposure experiments of C_{60}NWs

3.3.1. *Phagocytosis of C_{60}NWs*

Macrophages recognize, internalise and digest foreign materials. The uptake of them depends on their size and surface properties [5]. C_{60} is also phagocytized by macrophages [6] and the uptake rate of C_{60} is lower than that of graphite particles [7]. We observed that the macrophage-like cells gradually internalised C_{60}NWs after the exposure to C_{60}NWs with an inverted optical phase-contrast microscope (Fig.8). We will three-dimensionally locate the position of C_{60}NWs among the cells and study the phagocytosis of C_{60}NWs in more detail.

3.3.2. *Effect of C_{60}NWs' concentration and exposure period on the cell morphology.*

No alteration of cellular morphology was observed in the macrophage-like cells compared to the control group without exposure to C_{60}NWs after the exposure of 48 h for any concentration of C_{60}NWs in the observations by the inverted optical phase-contrast microscope (Fig.9). However, we are going to investigate the endpoints such as cell viability, cytokines, LDH and active oxygen generation in the next follow-up study using positive controls.

We cannot explain the fiber paradigm that a hazardous fibre is thinner than 3 μm in diameter, longer than 20 μm and biopersistent in the lungs [1] in the present paper dealing with only short (< 20 μm) C_{60}NWs. But some previous studies have reported that C_{60} (aggregate size was not described or larger than 1 μm) were nontoxic against mammalian cells [7, 8, 9] and dissolved inside lipid droplets in liver rats [10]. Owing to the weak van der Waals bonding forces acting between C_{60} molecules, C_{60}NWs may decompose into individual C_{60} molecules in living organisms. And on the basis of this assumption, C_{60}NWs may exhibit a biological effect like C_{60}. But these discussions are unclear now. We will carry out further researches on the digestion and dilution of C_{60}NWs using short and long C_{60}NWs.

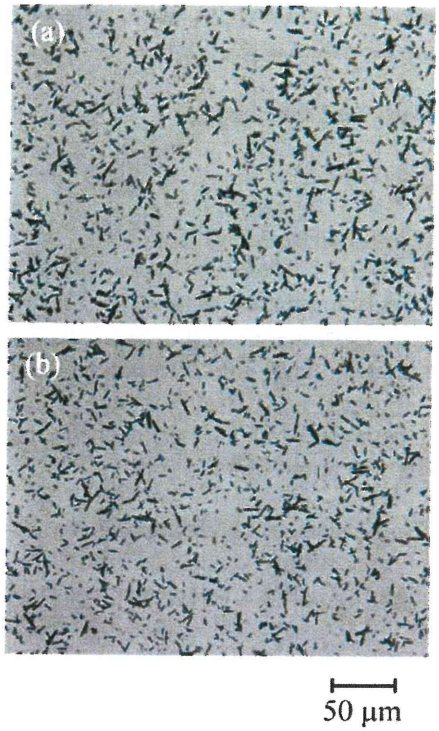

Figure 5. C_{60}NWs' dispersion in culture at a concentration of 10 μg/mL. (a) 1h and (b) 48 h after pouring the suspension of C_{60}NWs into the cell-free medium.

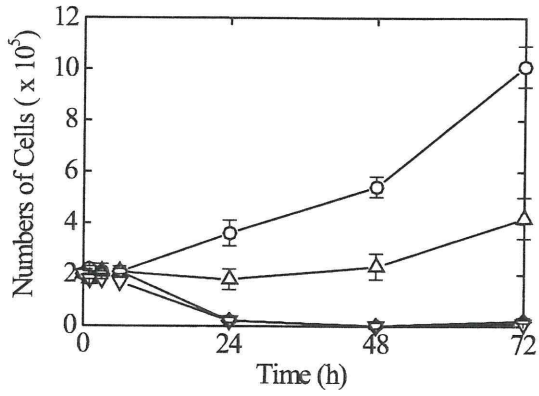

Figure 6. Suspended living cells after the PMA treatment. Circle, control (untreated); triangle, 1 nM PMA; diamond, 10 nM PMA; inverted triangle, 100 nM PMA. The results are expressed as the mean values for triplicate cultures with standard deviations.

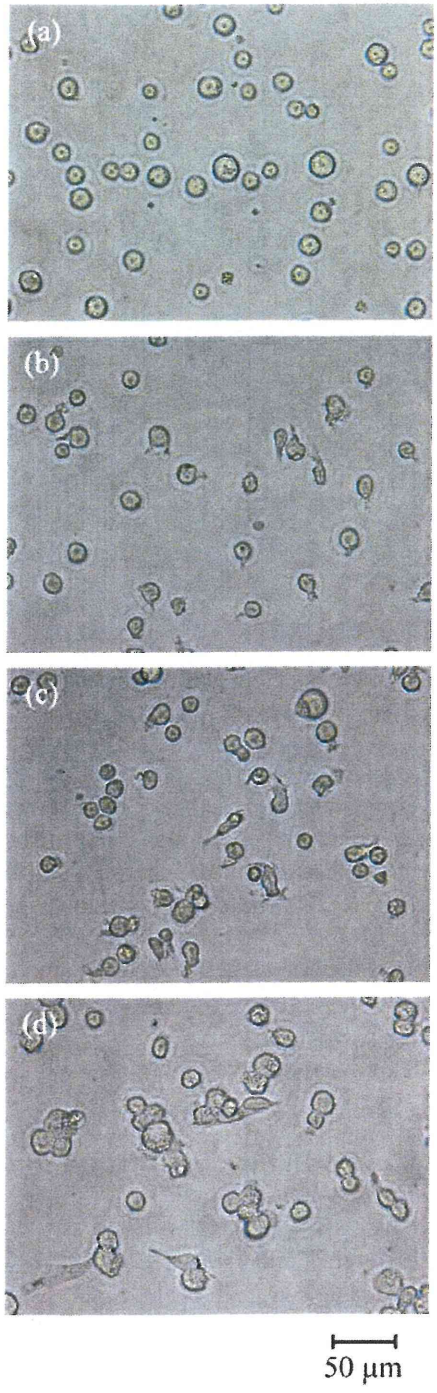

Figure 7. Morphological changes of THP-1 cells after (a) 1 h, (b) 3 h, (c) 6 h and (d) 24 h of 10 nM PMA treatment.

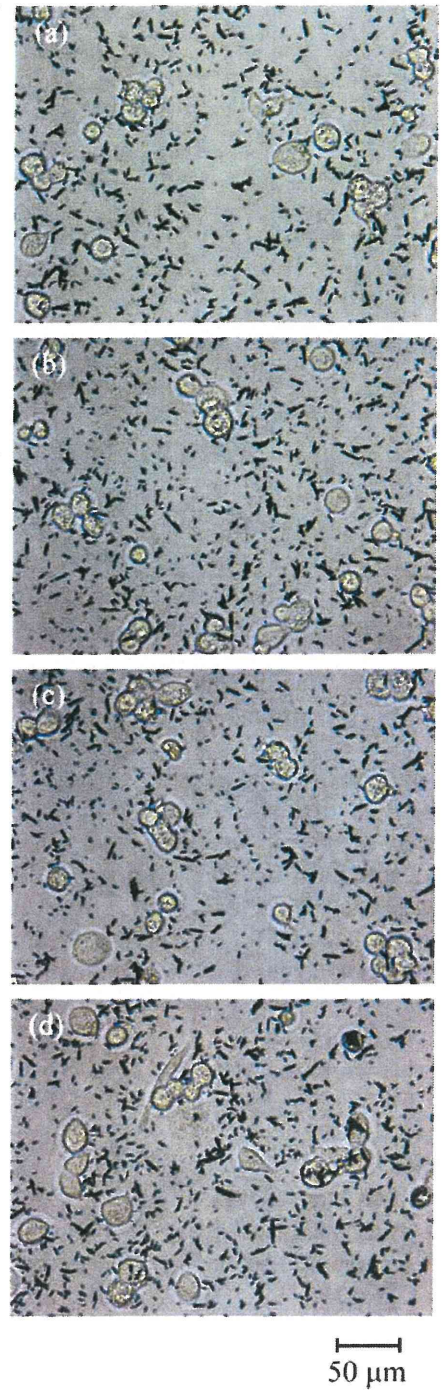

Figure 8. Macrophage-like cells exposed to C_{60}NWs for (a) 1 h, (b) 3 h, (c) 6 h and (d) 24 h at a concentration of 10 μg/mL.